Interconversion of Metarhodopsins I and II: A Branched Photointermediate Decay Model†

Martin Straume,‡ Drake C. Mitchell, James L. Miller,§ and Burton J. Litman*
Department of Biochemistry, University of Virginia Health Sciences Center, Charlottesville, Virginia 22908
Received March 15, 1990; Revised Manuscript Received July 9, 1990

ABSTRACT: Flash photolysis experiments designed to monitor the establishment of the metarhodopsin I to metarhodopsin II equilibrium are interpreted according to a branched model in which two spectrally indistinguishable but kinetically distinguishable forms of metarhodopsin II are postulated to exist in equilibrium with a common pool of metarhodopsin I. This interpretation arises from the consistent requirement for at least three exponentials for a valid description of the observed growth of absorbance at 380 nm following bleaching of bovine rhodopsin in rod outer segment disk membranes. Analysis of the 380-nm transient absorbance data permitted direct determination of the five physically interpretable individual rate constants of the model. This analysis represents a more explicit interpretation of kinetic data than that employed in earlier experiments of this kind, which involved estimating only apparent rates and apparent amplitudes of discrete multiexponential functions. The 380-nm absorbance contributions of all relevant species contributing to the observed dynamic absorbance change were accounted for simultaneously during nonlinear least-squares estimation of the model rate parameters. Analysis of deconvoluted equilibrium spectra acquired from samples identical with those used in the kinetics experiments confirmed the metarhodopsin I–metarhodopsin II equilibrium constants, K_{eq}, derived from the dynamic analyses. It is shown that K_{eq} varies from 1.28 at 10 °C to 7.3 at 37 °C and that ~90% of the metarhodopsin II present is in the form of metarhodopsin II_{slow} over the temperature range 10–37 °C. A physical interpretation of this decay model is discussed in the context of a distribution of metarhodopsin II structural and energetic states.

The visual pigment rhodopsin is an integral membrane protein that is converted to a physiologically active species by photon absorption. This form of rhodopsin binds and activates a peripheral guanine nucleotide binding regulatory protein (G_t)[1] in vertebrate retinal rod outer segments (Stryer, 1986). Such activation of G-proteins is now recognized as a widely occurring mechanism for transduction and regulation of biological information at membrane interfaces (Gilman, 1987). Activated G-proteins serve as signal transducers by specifically modifying the activity of at least one of a number of effector enzymes, thereby continuing the functional cascade of events initiated by a stimulus at a biological membrane (Allende, 1988). Rhodopsin and the other components involved in visual transduction in retinal rod outer segments therefore represent an important model biological system for elucidation of the mechanism of information regulation at membrane interfaces.

The decay of photolyzed rhodopsin involves sequential production of a series of spectrally distinguishable photointermediates (Ostroy, 1977). Production of meta II occurs on the correct time scale for involvement in photoactivated signal transduction in rod cells. Recent observations demonstrating enhancement of meta II formation by binding of G_t (Emeis et al., 1982) and the 48-kDa inhibitory protein arrestin also found in the rod outer segment (Schleicher et al., 1989) specifically support the involvement of meta II as the functionally relevant species in the rhodopsin spectral intermediate decay sequence. Meta II is therefore analogous to the agonist–receptor complex of other G-protein-activating receptor systems, and assumes a conformation capable of binding and activating G_t. The significance of understanding in detail the production of meta II is demonstrated by the fact that this process represents the formation of the functionally active form of a G-protein-activating receptor.

The lumi–meta I–meta II sequence of rhodopsin photointermediate decay has been examined by a number of laboratories since the initial report of Matthews et al. (1963) recognizing the existence of meta I and meta II as spectrally distinguishable species. However, these often comprehensive studies have consistently limited their kinetic interpretations to apparent amplitudes and apparent rate constants of discrete multiple exponential functions [see, for example, Applebury et al. (1974), Hoffmann et al. (1978), Litman et al. (1981), and Lewis et al. (1981)], although Parkes and Liebman (1984) have applied a somewhat higher order interpretation. We report here an explicit method of analysis with which to interpret the kinetics of establishment of the meta I–meta II equilibrium in mildly sonicated, bovine rod outer segment disk membranes. Measurements were performed over a range of temperatures and the rate constants determined from kinetic observations of absorbance changes at 380 nm. All of the individual rate constants and the contribution of each photointermediate to the absorbance at 380 have been determined at each temperature according to a branched meta I–meta II equilibrium model in which two spectrally indistinguishable, but kinetically distinguishable, meta II species are postulated to be in equilibrium with a common pool of meta I. The proposed model is the minimal model required to accurately characterize the observed absorbance growth data. The equilibrium constants derived from the kinetic analysis were

† Supported by NIH Grant EY00548 and NSF Grant PCM-8316858.
* Address correspondence to this author.
‡ Present address: Biocalorimetry Center, Department of Biology, The Johns Hopkins University, Baltimore, MD 21218.
§ Present address: Department of Physiology, University of California, San Francisco, San Francisco, CA 94143.

[1] Abbreviations: G_t, visual G-protein, transducin; meta II, metarhodopsin II; meta I, metarhodopsin I; lumi, lumirhodopsin; DTPA, diethylenetriaminepentaacetic acid; PIPES, piperazine-*N*,*N*′-bis(ethanesulfonic acid); DTT, dithiothreitol; ROS, outer segment of the retinal rod cell.

0006-2960/90/0429-9135$02.50/0

identical with those obtained from independent measurements of deconvoluted meta I–meta II equilibrium spectra obtained under the same experimental conditions. The results and implications of this proposed model are discussed in the context of a distribution of meta II structural and energetic states. In the following paper in this issue (Mitchell et al., 1990), this interpretative model is used to address the influence of cholesterol-induced ordering of bilayer lipids on the meta I–meta II equilibrium in synthetic, rhodopsin-containing egg phosphatidylcholine vesicles of varying cholesterol content.

Experimental Procedures

Isolation of Rod Outer Segment Disk Membranes. Native bovine rod outer segment disk membranes were isolated by the Ficoll floatation method as described by Smith et al. (1975) except that all buffers and solutions were extensively degassed with argon and contained 50 μM DTPA and 62.5 μM $MgCl_2$ to minimize sample oxidation induced by trace amounts of iron. This isolation procedure includes washing with hypotonic buffer, which is the accepted method for removing residual transducin bound to disks (Kuhn, 1981). Total phospholipid content was determined by phosphate analysis according to the method of Bartlett (1959). Total protein content was estimated by the method of Lowry et al. (1951). Unbleached rhodopsin content was quantified by monitoring the change in 500-nm absorbance resulting from complete bleaching of detergent-solubilized samples. The 280-to-500 nm absorbance ratio was also determined as an index of the quality of isolated disks [see Straume and Litman (1988) and references cited therein]. Samples for both flash photolysis and equilibrium measurements were prepared by first dialyzing concentrated suspensions of isolated disks against 10 mM PIPES (pH 7.0), 60 mM KCl, 20 mM NaCl, 2 mM $MgCl_2$, 2 mM DTT, and 0.05 mM DTPA (pH 7.0 PIPES buffer). This concentrated stock was then diluted approximately 1:10 into appropriate temperature-compensated PIPES buffer to yield samples of 0.35–0.5 mg mL^{-1} rhodopsin. Dilution into these temperature-compensated buffers was performed so that sample pH was invariantly 7.0 for each temperature at which data were collected (10, 20, 30, and 37 °C). These samples were next sonicated at low power under argon for 90 s in a bath sonifier filled with water at 0 °C.

Flash Photolysis Measurements. Kinetic absorption data were acquired by using a flash photolysis system of our own design [for a review of flash photolysis instrumentation, see Lozier (1982)]. The sample was contained in a 1-mL quartz curvette of 1-cm path length. The curvette was positioned tightly in a channeled, thermostated aluminum block, the temperature of which was regulated to ±0.2 °C with a circulating water bath. The photolyzing flash was generated by a flash lamp-pumped dye laser. The laser was equipped with Coumarin 504 dye and tuned to 503 nm, and the full width at half-maximum of the photolyzing flash was approximately 280 ns. The laser pulse was horizontally polarized as emitted from the laser tube. In order to ensure uniformly horizontally polarized laser emission, the beam was passed through a horizontally oriented polarizer prior to encountering a pellicle beam splitter that reflected 10% of the laser flash into the sample cuvette. The actinic flash traversed the sample such that it was collinear with the monitoring beam. The monitoring beam source was a small 50-W metal–halide lamp powered by a heavy-duty 12-V battery. An electronic shutter was in place in front of the monitoring beam lamp and was opened approximately 1 s before photolysis of the sample. In this way, sample exposure to the monitoring beam was minimized, but the photomultiplier was exposed for a sufficient time to produce steady preflash output. The monitoring beam was first passed through a 6-cm water filter to remove infrared radiation. It then traveled through a 380-nm interference filter with a 2-nm band-pass. A polarizing filter was next in the path and oriented the polarization of the monitoring beam at an angle of 54.7° to that of the horizontally polarized photolyzing laser beam. This "magic angle" relative orientation of the actinic and monitoring beams permitted direct observation of accurate amplitude information from transient absorbance changes of photoactive species in randomly oriented samples (Lozier, 1982). Beyond this polarizer was a pellicle beam splitter which passed 90% of the monitoring beam intensity to a lens that focused the beam through the sample cuvette. A lens situated beyond the sample directed the beam through another 380-nm interference filter in series with a Corning glass filter (75-9) prior to impinging on a Hammamatsu R928 photomultiplier tube. These last two filters shielded the photomultiplier from the actinic laser pulse. The current output of the photomultiplier was converted to voltage and amplified by a photometric amplifier with a minimum time constant of 15 μs. This voltage signal was digitized and stored on a computer interfaced for complete instrument control and data acquisition.

A few milliliters of sample was prepared immediately before measurements were performed and kept on ice under argon. A 200-μL aliquot was placed into the sample cuvette, and temperature equilibration was achieved in less than 2 min. Following a single laser flash, the partially bleached sample (typically approximately 20%) was removed from the cuvette and stored on ice under argon. Measurements were made on 5–10 aliquots at each temperature per experiment. All results reported are the average of 3–4 separate disk preparations and flash experiments. The initial unbleached rhodopsin concentration of the original samples and the fraction bleached by the laser flash were determined for each aliquot by measuring the change in 500-nm absorbance resulting from complete bleaching of the aliquots after detergent solubilization.

Analysis of Flash Photolysis Data. The change in transmitted intensity of the monitoring beam as a function of time was determined relative to the preflash intensity. The observed change in intensity was converted to absorbance by the use of calibrated dye solutions, the absorbance of which was determined on a dual-beam spectrophotometer. Response was found to be linear over the range of light intensities used and consistent with that predicted theoretically. No bleaching of samples by the monitoring beam could be detected at any of the temperatures examined as determined from parallel experiments in which the actinic laser flash was absent (a total of approximately 1–2 s of sample exposure to the monitoring beam). A total of 5000 data points were typically collected over 3–4 decades of time at a maximum resolution of 5 μs. These acquired data were reduced to approximately 350 data points evenly spaced in log time by application of a digital moving boxcar filter, averaging not more than 9 consecutive observed values. Five to ten of these reduced data files, representing flash experiments on replicate aliquots at each temperature, were then averaged to produce a final data file used in analysis. Reproducibility among these replicate measurements was excellent as indicated by the nearly identical fractions of rhodopsin bleached by the actinic pulses, as well as their associated magnitudes of 380-nm absorbance growth.

Nonlinear least-squares analysis of data was performed by using the modified Gauss–Newton algorithm developed by Johnson (Johnson, 1983; Johnson & Frasier, 1985). All analysis was performed on a DEC LSI 11/73 computer. The

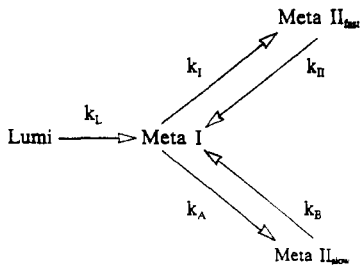

FIGURE 1: Branched meta II model employed to analyze all kinetic observations of photoinduced 380-nm absorbance transients is schematically presented. The five rate constants, the extinction coefficients at 380 nm of all species, and the amount of rhodopsin bleached are the parameters necessary to fully characterize the observed dynamic data according to this model.

scatter in 200 preflash base-line points collected immediately before exposure of the sample to the laser pulse was used to estimate the uncertainty (i.e., standard deviation) inherent to the observed data. This uncertainty was propagated through all averaging processes (i.e., digital filtering of original files and averaging to the final record), and appropriate, independent assignments of uncertainty were given to each final point. This permitted calculation of the reduced variance of fit (reduced χ^2 value) to aid in defining the statistical validity of any given model-dependent least-squares parameter estimation process.

Comparison of the reduced χ^2 values resulting from double- and triple exponential analyses of the kinetic data by way of the F-test clearly demonstrated the statistical superiority of the triple-exponential approximation (see Results). Higher order models were not statistically justified in that the variance of fit was not significantly improved. This observation, as well as those of other investigators suggesting the inadequacy of double-exponential approximations (Lewis et al., 1981; Hoffmann et al., 1978), led us to consider the kinetic data according to the branched meta II model presented in Figure 1. The time scale over which the kinetic data were acquired made it unnecessary to consider species prior to lumi and beyond meta II in the rhodopsin photointermediate decay cascade. The solution of the system of linear first-order differential equations characteristic of the decay scheme shown in Figure 1 predicts triple-exponential behavior with six unknown model-fitting parameters: the five rate constants k_L, k_I, k_{II}, k_A, and k_B as well as a parameter defining the extinction of meta I at 380 nm relative to that of rhodopsin at 498 nm, $\epsilon_{MI}(380)/\epsilon_{rho}(498)$. The rate constants k_I and k_{II} define the rapidly interconverting meta I $\leftrightarrow$ meta II_{fast} equilibrium, and k_A and k_B define the more slowly interconverting meta I $\leftrightarrow$ meta II_{slow} equilibrium. The extinction coefficients of both meta II_{fast} and meta II_{slow} were assumed identical and equal to 38 000 cm^{-1} M^{-1} (Applebury, 1984). Attempts at analysis while allowing the fractional contribution of lumi to the observed 380-nm absorbance increase to vary consistently yielded values which were approximately zero (less than 0.1%). This result is consistent with the small difference in absorbance at 380 nm between lumi and rhodopsin and the temporal resolution of the the data acquisition instrumentation. Implementation of this model in analysis, therefore, was performed by fixing at zero the contribution of lumi to the observed increase in absorbance at 380 nm. Independent determination of the total amount of rhodopsin bleached by the actinic pulse, as described above, made it possible to fully define the system.

For each data set, most probable values were determined for each of the model parameters as were their associated upper and lower confidence intervals corresponding to one standard deviation (68.3% confidence). Equilibrium constants

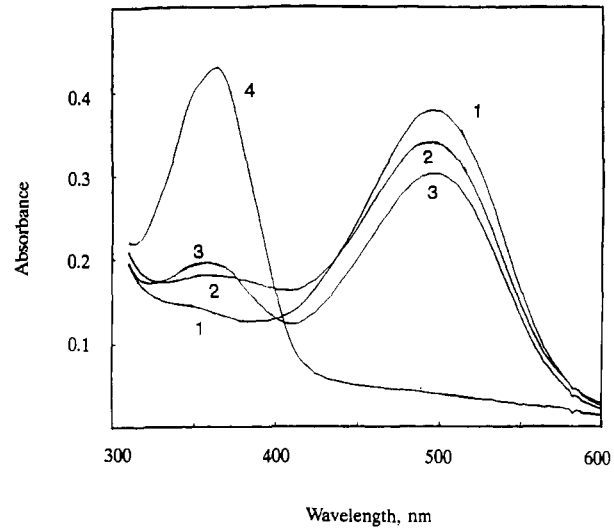

FIGURE 2: Example of the set of four successive absorbance spectra acquired for determination of the overall meta I–meta II equilibrium. These spectra of mildy sonicated disk membranes in pH 7.0 PIPES buffer were obtained at 30 °C on a Hewlett-Packard 8452A diode array spectrophotometer. The sample was first scanned before bleaching (1), after partial bleaching by exposure to a strobe flash (2), following addition of hydroxylamine to the partially bleached sample (3), and after complete bleaching of the sample in the presence of hydroxylamine (4).

defining each branch of the meta I–meta II equilibrium and the overall meta I–meta II interconversion were calculated from the estimated model rate constants. Uncertainties in these equilibrium constants were linearly propagated from those of the individual rate constants.

Equilibrium Spectral Measurements. Equilibrium absorbance spectra of aliquots of the same disk membrane samples used for kinetic measurements were obtained at the same temperatures employed for the kinetic studies. Measurements were made on both a Varian 210 dual-beam spectrophotometer and a Hewlett-Packard 8452A diode array spectrophotometer. Two milliliters of sample was placed into a 3-mL cuvette housed in a thermostated cuvette holder and stirred continuously with a small magnetic stir bar. Temperature was regulated with a circulating water bath to within 0.2 °C of the desired value. An empirically closely matched scattering blank was placed in the reference beam of the Varian 210. A similar suspension was used to acquire a stored reference spectrum on the Hewlett-Packard 8452A. Perfect matching of the reference with the sample was not possible; however, the nature of the protocol and analysis to be described implicitly accounted and corrected for imperfect scattering references.

After temperature equilibrium had been achieved, a series of four absorbance spectra between 310 and 650 nm were acquired. The Hewlett-Packard 8452A spectrophotometer obtained complete spectra in 0.3 s, which typically bleached less than 0.3% of the sample. Scans in the Varian 210 were performed at 10 nm/s, the most rapid rate available, spanning 34 s. Data at 37 and 30 °C were obtained only with the Hewlett-Packard 8452A because the decay of meta II during acquisition of spectra was significant in the Varian 210 at these temperatures. Results obtained at 20 and 10 °C were essentially identical whether acquired on the Varian 210 or the Hewlett-Packard instrument. An example of the four spectra is presented in Figure 2. The first spectrum recorded (1) was that of the initial, unbleached sample. The second spectrum (2) was taken immediately following exposure of the sample to a single flash from a Metz 451 camera strobe passed through a 500-nm interference filter of 25-nm band-pass.

Bleach levels between 20 and 25% (the same fractions bleached observed in the kinetic experiments) were typically obtained. The third spectrum (3) was acquired after addition of 20 μL of 2 M hydroxylamine at pH 7.0. The hydroxylamine was freshly prepared, and separate aliquots were adjusted to pH 7.0 at the temperature of the measurement. The fourth spectrum (4) was obtained after complete bleaching of the sample by exposure to a high-intensity lamp for 60 s. A microcomputer interfaced to the Varian 210 acquired spectra at 2-nm resolution, the same resolution as the Hewlett-Packard. The digitized data was then transferred to a DEC LSI 11/73 computer for analysis.

Analysis of Equilibrium Spectral Data. The four spectra obtained as described above collectively contained varying contributions from four spectrally distinct species: rhodopsin, meta I, meta II, and retinal oxime. No other rhodopsin photointermediates contributed to the observed spectra given the time scales and conditions involved in the measurments. The first spectrum (1) contained contributions from rhodopsin only (~498-nm absorbance maximum). After being partially bleached with the strobe flash, the second spectrum (2) contained contributions from the remaining unbleached rhodopsin as well as meta I and meta II in equilibrium (~478- and ~380-nm absorbance maxima, respectively). Addition of hydroxylamine at this point left the unbleached rhodopsin intact, but converted the meta I and meta II to opsin (rhodopsin with no associated retinal chromophore) and free retinal oxime (λ_{max} ~363 nm) (spectrum 3). After total bleaching, retinal oxime was the only species contributing to the absorbance in spectrum 4.

The first step in the analysis was to generate the three possible difference spectra from (1), (3), and (4). These spectra contained contributions from rhodopsin and retinal oxime only. The differences were taken such that the rhodopsin spectrum was inverted, i.e., a negative difference peak. By use of such difference spectra in the analysis, any contributions from scattering in the original spectra were automatically eliminated, assuming minimal scattering changes upon bleaching. These three difference spectra were analyzed by simultaneously fitting asymmetric quasi-Gaussian functions of the type given in the equation:

$$A(\lambda)_n = f_n A_{ox}\{\exp(-[(|1/\lambda - 1/\lambda_{ox}|/W_{ox,l})^{P_{ox,l}}]) + \exp(-[(|1/\lambda - 1/\lambda_{ox}|/W_{ox,h})^{P_{ox,h}}])\} - f_n A_{rho}\{\exp(-[(|1/\lambda - 1/\lambda_{rho}|/W_{rho})^{P_{rho,l}}]) + \exp(-[(|1/\lambda - 1/\lambda_{rho}|/W_{rho,h})^{P_{rho,h}}])\} \quad (1)$$

The subscript "n" (n = 1, 2, 3) in eq 1 differentiates between the three separate difference spectra, and the parameters f_n account for differences in the amount of rhodopsin and retinal oxime present in the three spectra. The difference spectrum (4) − (1) contains all of the original rhodopsin and all of the final retinal oxime; therefore, f_1 = 1. The difference spectrum (3) − (1) contains only the rhodopsin bleached by the strobe flash and the corresponding amount of retinal oxime; thus, f_2 = fraction bleached. The difference spectrum (4) − (3) contains the residual unbleached rhodopsin and the corresponding retinal oxime; thus, f_3 = 1 − (fraction bleached). The remaining parameters in eq 1 describe the shape and location of the rhodopsin and retinal oxime absorption bands. The first two terms of eq 1 give the location and shape of the retinal oxime absorption band; the last two terms give the location and shape of the inverted rhodopsin absorption band. A_i is the absorbance of species i at its wavelength of maximum absorbance, λ_i. $W_{i,l}$ and $P_{i,l}$ characterize the width and powder dependence of species i at wavelengths lower than its peak maximum, respectively. Similarly, $W_{i,h}$ and $P_{i,h}$ characterize the width and power dependence of species i at wavelengths higher than its peak maximum, respectively. The accommodation of peak asymmetry and non-Gaussian shape by the functional form used here is consistent with the fact that electronic absorption bands consist of envelopes composed of numerous subbands and are generally not expected to be symmetric or Gaussian (Metzler et al., 1986). Single values of these parameters were determined by simultaneously fitting the appropriate three equations of the type given in eq 1 to the three difference spectra.

After determination of the parameters characteristic of the rhodopsin and retinal oxime absorbance profiles, the three possible difference spectra containing meta I and meta II contributions were generated [(2) − (1), (2) − (3), and (2) − (4)]. The contributions of rhodopsin and/or retinal oxime were subtracted from these difference spectra based on the results derived above for rhodopsin and retinal oxime peak shapes and fraction bleached. This produced three spectra which contained only the meta I and meta II absorbance profiles. An asymmetric, quasi-Gaussian function of the form presented in eq 1 was then used to estimate those parameters (A_i, λ_i, $W_{i,l\text{ and }h}$, and $P_{i,l\text{ and }h}$) characteristic of meta I and meta II by globally considering these three corrected difference spectra. These three spectra were generally nearly identical, and were averaged to form the final deconvoluted meta I–meta II equilibrium spectrum. Concentrations of meta I and meta II were then calculated on the basis of an extinction coefficient for meta I of 44 000 M^{-1} cm^{-1} and for meta II of 38 000 M^{-1} cm^{-1} (Applebury, 1984). Asymmetric confidence intervals were estimated for the derived meta I and meta II concentrations at confidence levels corresponding to one standard deviation (68.3% confidence), but because of the minimal observed asymmetry, a single estimate of standard deviation is reported.

Results

The inability of a double-exponential approximation to adequately describe the flash-induced rise in 380-nm absorbance observed from mildly sonicated bovine rod outer segment disk membranes at pH 7.0 and 10 °C is demonstrated in Figure 3. The change in absorbance is plotted versus log time, and inspection of the residuals shown in the insets clearly demonstrates that two exponentials are insufficient to describe the data, whereas a triple-exponential model eliminates nearly all the "ringing" in the residuals. In addition, the variance of fit improves by a factor of more than 3.7, a highly significant change. A similar requirement of three exponentials to accurately represent the observed dynamic 380-nm absorbance growth was found at all of the temperatures examined. The slowest of the three apparent rate constants was much greater than that observed for transducin-dependent meta II formation (unpublished results; Emeis et al., 1982), making it improbable that interaction with residual transducin was responsible for the complicated kinetics which necessitate a third exponential term. This possibility is further ruled out by the fact that identical triple-exponential behavior is also observed in recombinant vesicles where chromatographic purification of rhodopsin has removed all transducin (Mitchell et al., 1990). Attempts to further improve the fits by applying four exponentials failed to produce statistically significant reductions in the variances of fit at any temperature. These findings are consistent with the branched meta II model, which reduces to a triple-exponential function.

Table I: Derived Branched Meta II Model Parameters[a]

parameter	temp (°C) 37	30	20	10
k_L	4.9 (0.8)	1.79 (0.24)	0.78 (0.12)	0.37 (0.05)
k_I	0.34 (0.03)	0.073 (0.018)	0.0236 (0.0010)	0.00313 (0.00007)
k_{II}	0.52 (0.18)	0.14 (0.03)	0.061 (0.004)	0.0247 (0.0004)
k_A	0.484 (0.024)	0.130 (0.007)	0.0228 (0.0009)	0.00349 (0.00010)
k_B	0.072 (0.005)	0.033 (0.005)	0.0119 (0.0006)	0.00303 (0.00011)
$\epsilon_{MI}(380)/\epsilon_{rho}(498)$	0.32 (0.07)	0.266 (0.017)	0.111 (0.017)	0.0418 (0.0022)

[a] Rate constants are reported in units of ms^{-1}; all rate constants, k_i, are defined by the schematic representation of the branched meta II model presented in Figure 1; $\epsilon_{MI}(380)/\epsilon_{rho}(498)$ is the ratio of meta I extinction at 380 nm to that of rhodopsin at 498 nm. Values in parentheses are estimated standard deviations.

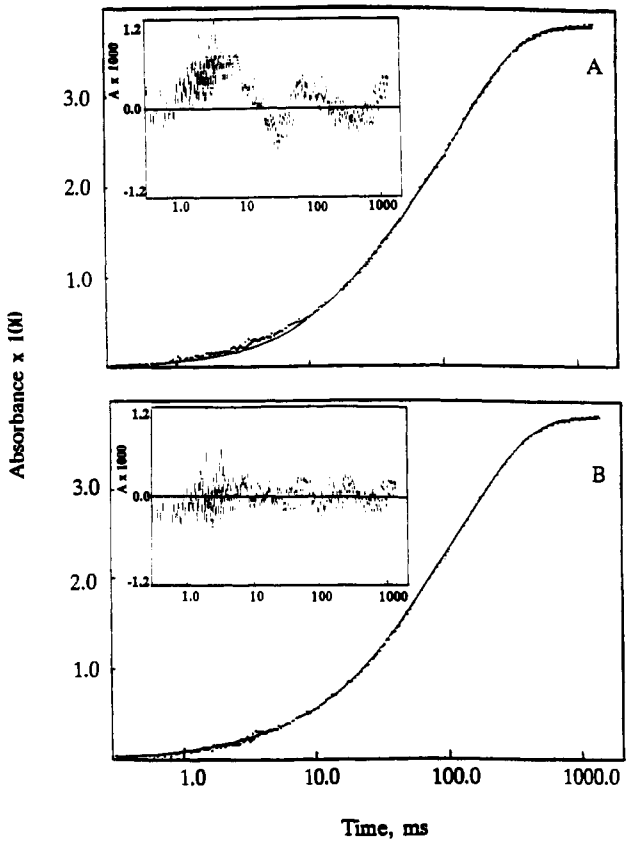

FIGURE 3: Example of the results of discrete double (A) and triple (B) exponential analysis, with corresponding residuals (inset), of the 380-nm absorbance transient obtained from laser flash photolysis of mildly sonicated disk membranes at pH 7.0 and 10 °C. The plots are presented in log time. The variance of fit was reduced by a factor of 3.7 on going from the double- to the triple-exponential function.

The rate constants derived from application of the branched meta II model to the kinetic measurements are presented in Table I for all four temperatures considered in this work. The most probable derived values for each of the model parameters are presented [k_L, k_I, k_{II}, k_A, k_B, and $\epsilon_{MI}(380)/\epsilon_{rho}(498)$] along with an estimate of the uncertainty (standard deviation) associated with each one. Confidence intervals were actually derived as asymmetric upper and lower limits at 68.3% confidence (equivalent to one standard deviation) for each model parameter, but the observed asymmetry was never greater than approximately 10%. Therefore, reported in Table I are single estimates of the standard deviation calculated as half of the total confidence interval range. The overall and individual branch equilibrium constants, as calculated from the rate constants, are reported in Table II. Uncertainties were linearly propagated for these quantities from those of the appropriate constituent rate constants.

Table II: Equilibrium Constants Derived from Analysis of Kinetic and Equilibrium Data[a]

parameter	temp (°C) 37	30	20	10
$K_{eq,total}$(kinetic)	7.3 (0.6)	4.4 (0.7)	2.31 (0.13)	1.28 (0.05)
$k_{eq,fast}$	0.66 (0.24)	0.52 (0.17)	0.39 (0.03)	0.127 (0.003)
$K_{eq,slow}$	6.7 (0.6)	3.9 (0.7)	1.92 (0.12)	1.15 (0.05)
$K_{eq,total}$(equil)	8.1 (0.9)	4.6 (0.7)	2.32 (0.08)	1.45 (0.18)

[a] $K_{eq,total}$(kinetic) is the overall meta I–meta II equilibrium constant as determined from kinetic data; $K_{eq,fast}$ and $K_{eq,slow}$ are the equilibrium constants for the meta I–meta II equilibria characteristic of the respective individual branches of the proposed branched meta II model; $K_{eq,total}$(equil) is the equilibrium constant for the overall meta I–meta II equilibrium as determined from the equilibrium absorbance measurements. Values in parentheses are estimated standard deviations.

Table III: Derived Activation Parameters for the Rate Constants of the Branched Meta II Model[a]

parameter	k_L	k_I	k_{II}	k_A	k_B
$\Delta H^\ddagger$ (kcal mol^{-1})	15 (3)	29.0 (1.8)	14.7 (1.9)	31.0 (0.5)	20.3 (0.8)
$\Delta S^\ddagger$ (cal K^{-1} mol^{-1})	7 (10)	46 (6)	0 (6)	53.4 (1.2)	16 (3)

[a] Activation enthalpies ($\Delta H^\ddagger$) and entropies ($\Delta S^\ddagger$) were determined by nonlinear least-squares estimation to eq 2 of the temperature dependence of the derived branched meta II model rate parameters presented in Table I (weighted by their associated standard deviations). Values in parentheses are estimated standard deviations.

The observed decline of all of the derived model rates as temperature decreases is consistent with predictions of reaction rate theory (Arrhenius behavior). A summary of all of the derived activation enthalpies and entropies is presented in Table III as obtained from application of the following expression to the temperature dependence for each of the rate constants:

$$k = k_B T/h \exp(\Delta S^\ddagger/R) \exp(-\Delta H^\ddagger/RT) \qquad (2)$$

where k_B is Boltzmann's constant, T is absolute temperature, h is Planck's constant, R is the universal gas constant, $\Delta S^\ddagger$ is the activation entropy, and $\Delta H^\ddagger$ is the activation enthalpy. The activation parameters characteristic of the rate constants presented in Table I (weighted by their associated derived uncertainties) were each determined by nonlinear least-squares estimation directly with eq 2, i.e., the activation parameters were not obtained from fitting to a linearized transform of eq 2. The standard deviations reported in Table III are single estimates of derived uncertainty (at 68.3% confidence) which disregard the small inequivalency between the upper and lower derived confidence intervals.

To most clearly demonstrate the behavior of each of the model rates with respect to temperature, plots of log (k_i/T) versus $1000/T$ (the linearized form of eq 2) are presented in

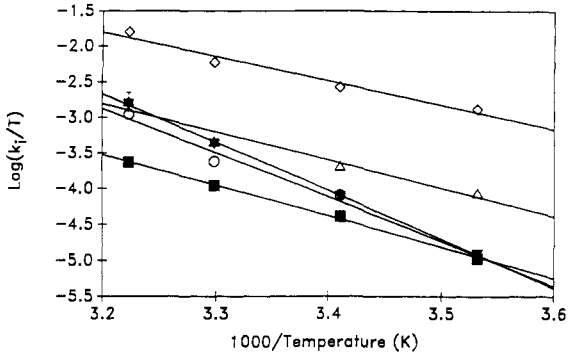

FIGURE 4: Temperature dependence of the rate constants of the branched meta II model: k_L (◇), k_I (○), k_{II} (△), k_A (▼), k_B (■).

Table IV: Changes in Total ΔH, ΔS, and ΔG_{25} for Meta II_{fast}, Meta II_{slow}, and Meta II_{total}[a]

parameter	meta II_{fast}	meta II_{slow}	meta II_{total}
ΔH (kcal mol^{-1})	10.7 (2.0)	10.2 (0.9)	10.6 (0.5)
ΔS (cal K^{-1} mol^{-1})	33.7 (6.7)	36.5 (3.0)	37.9 (1.8)
ΔG_{25} (kcal mol^{-1})	0.62 (0.10)	−0.62 (0.04)	−0.70 (0.03)

[a] Changes in total enthalpy (ΔH), entropy (ΔS), and free energy at 25 °C (ΔG_{25}) were determined by nonlinear least-squares parameter estimation to eq 3 of the temperature dependence of the appropriate equilibrium constants (weighted by their associated uncertainties). Values in parentheses are estimated standard deviations.

Figure 4. It is immediately apparent that all five model rate constants exhibit Arrhenius-type temperature dependence. The activation enthalpies of the two forward meta I to meta II rate constants (k_I and k_A) are similar and of greater magnitude (as indicated by steeper slopes) than are those of the other model rate parameters (k_L, k_{II}, and k_B), all three of which display similar activation enthalpies (i.e., similar slopes; see also Table III). Readily apparent from Figure 4 is that the forward rate constants for each branch of the proposed model (k_I and k_A) are approximately equal at all temperatures but that the reverse rates (k_{II} and k_B) are quite different. It is therefore the difference in reverse rate constants for the two proposed branches of the meta I–meta II interconversion which is primarily responsible for the difference in equilibrium constants derived for the two branches.

The difference between meta II_{fast} and meta II_{slow} was also examined by determining the changes in ΔS and ΔH for these two proposed states relative to meta I using eq 3 where

$$K_{eq,species} = \exp(\Delta S_{species}/R) \exp(-\Delta H_{species}/RT) \quad (3)$$

"species" refers to meta II_{fast}, meta II_{slow} or meta II_{total} and ΔH and ΔS are the changes in enthalpy and entropy, respectively, relative to meta I. Changes in free energy at 25 °C, ΔG_{25}, were determined by using an equation similar to eq 3 where ΔS was exchanged for the quantity $(\Delta H - \Delta G_{25})/298.15$. This provides for direct estimation of confidence intervals for each parameter of interest. The results of this analysis are given in Table IV and show that the large difference between $K_{eq,fast}$ and $K_{eq,slow}$ is due to small relative differences in both ΔS and ΔH. At 25 °C, the free energy difference between the two is only about 1.3 kcal mol^{-1} as shown in Table IV. The difference in relative enthalpy is ca. 0.5 kcal mol^{-1}, and the difference in relative entropy accounts for the other ca. 0.8 kcal mol^{-1}. Thus, the more slowly interconverting branch clearly favors formation of meta II to a much greater extent than does the more rapidly interconverting branch, but they exhibit somewhat similar dependence with temperature. This is not surprising given the nearly parallel temperature-dependent behavior (i.e., nearly equivalent activation enthalpies) of the forward (k_I and k_A) and reverse

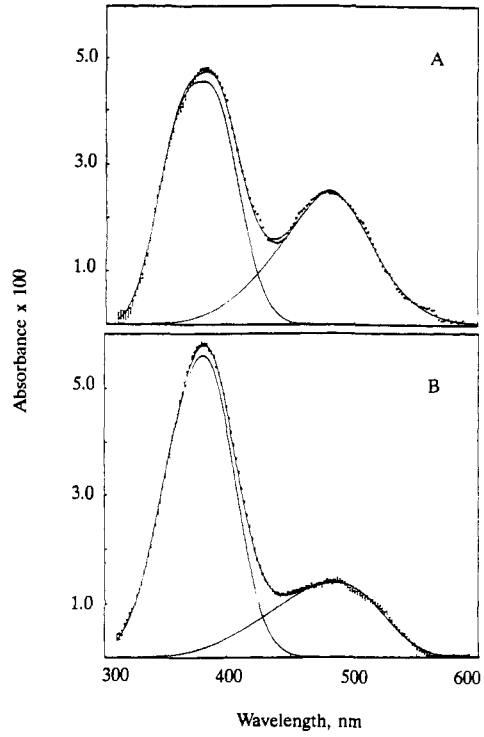

FIGURE 5: Examples of the deconvoluted equilibrium spectra of meta I and meta II in mildly sonicated disk membranes at pH 7.0 obtained at 20 °C (A) and 30 °C (B), along with the individual derived meta I and meta II spectra. See Analysis of Equilibrium Spectral Data under Experimental Procedures for the details of how these difference spectra were derived from sets of absorbance spectra of the type shown in Figure 2.

(k_{II} and k_B) rate constants in Figure 4 (see also Table III).

The values of the equilibrium constants for the meta I–meta II interconversion derived from the kinetic data are confirmed by analysis of the deconvoluted equilibrium spectra obtained from these same samples. Examples of the equilibrium absorbance spectra derived for these midly sonicated disk membranes at 20 and 30 °C at pH 7.0 are shown in panels A and B, respectively, of Figure 5. The redistribution of the meta I–meta II equilibrium in favor of meta II as temperature is increased is clearly demonstrated. Close inspection of the meta I bands in these two figures shows that a second effect of increased temperature is a preferential broadening of the blue side of the meta I band. At all four temperatures examined, the overall equilibrium constants derived from kinetic experiments agreed with those determined from the deconvoluted equilibrium spectra (see Table II).

Discussion

We report here explicit derivation of all of the individual rate constants characteristic of establishment of the meta I–meta II equilibrium in the spectral intermediate decay sequence of photolyzed bovine rhodopsin. The consistent requirement of triple-exponential decay kinetics to accurately characterize the transient growth of 380-nm absorbance prompted development of the branched meta II model presented here (see Figures 1 and 3). Attempts to model the kinetic observations using two kinetically distinct meta I species failed to provide accurate or physically meaningful characterization of the dynamic observations. This is not surprising considering that the kinetic complexity which dictates a third exponential term is present in the latter portion of the kinetic data, while the fastest process observed, formation of meta I from lumi, is well characterized by a single exponential. Thus, this is the minimal model capable of simultaneously accounting

for the kinetic data, as well as the equilibrium spectra obtained under identical conditions.

Earlier kinetic studies on the lumi–meta I–meta II time scale for bovine rhodopsin in its native membrane environment have demonstrated the presence of triple-exponential behavior in this system (Lewis et al., 1981; Hoffmann et al., 1978) although some reports of biexponential behavior have also been published (Applebury et al., 1974; Litman et al., 1981). Analysis of this dynamic response has been largely limited to the domain of apparent rate and amplitude parameters (Applebury et al., 1974; Hoffmann et al., 1978; Litman et al., 1981; Lewis et al., 1981). Nevertheless, much has been implied about the temperature and pH dependence of metarhodopsin kinetics and spectral properties from interpretation of such apparent parameters (Hoffmann et al., 1978; Lewis et al., 1981). Parkes and Liebman (1984) have attempted to deconvolve this equilibrium into its consistuent rate constants, although they considered this phenomenon in a manner consistent with only double-exponential behavior.

Solution of the linear, first-order differential equations descriptive of the branched meta II model yields analytical expressions reducible to the form of a discrete triple exponential. The preexponential factors obtained in this way are equivalent to the apparent amplitudes considered in prior studies. Expressions equivalent to the apparent rate constants derived in earlier examinations may also be defined. The complexity of these expressions, however, immediately makes apparent the challenges involved in trying to extract precise physical interpretations about the dynamic behavior of the meta I–meta II transition from consideration of apparent amplitudes and rate constants.

In the present study, the lumi–meta I–meta II decay sequence was interpreted by considering individual forward and reverse rates obtained from application of the branched meta II model to observations of 380-nm absorbance transients. The kinetic behavior derived from these experiments is consistent with decay of a single pool of meta I through a single activated intermediate which then decays to form two energetically distinguishable (and therefore kinetically distinguishable) but spectrally indistinguishable forms of meta II. The nearly superimposable plots of log k_I and log k_A versus $1000/T$ in Figure 4 are consistent with the interpretation of a single pool of meta I decaying through a single activated intermediate form to meta II, because the derived forward rates are nearly equal for both branches of the proposed model. The properties of the reverse reaction are also illustrated in Figure 4, in the parallel but clearly vertically displaced plots of log k_{II} and log k_B versus $1000/T$. This is consistent with two energetically different forms of meta II passing through a common activated intermediate state on the path to forming meta I.

Similar conclusions regarding the existence of two, discrete, kinetically distinguishable forms of the M spectral intermediate in the bacteriorhodopsin photocycle have been reported by several investigators [for a review, see Stoeckenius and Bogomolni (1982)]. Several kinetic studies of the M intermediate in bacteriorhodopsin have indicated the existence of two distinct population, M^f and M^s, and there has been a report of a functional difference between M^f and M^s (Li et al., 1984). The separate, distinct absorption spectra of these two species have been reported by Dancshazy et al. (1988). These authors had additional experimental observations in the form of fast time-resolved absorbance spectra which indicated that the two forms of M had somewhat different absorbance profiles. In the present study, absorbance profiles of meta I and meta II were also considered, but not at acquisition rates equivalent to those of the kinetic observations at 380 nm. No indications of multiple spectral forms of meta II were apparent from these measurements; however, the possibility of subtle differences in the absorbance profiles of the proposed fast and slow forms of meta II cannot be addressed given the temporal resolution and precision of the derived meta I and meta II absorbance spectra.

Implicit to the rigorous kinetic and equilibrium spectral analysis is accommodation of any temperature-dependent changes in spectral properties of the relevant species. The increase in the relative extinction of meta I at 380 nm with increasing temperature obtained from the kinetic analysis is summarized in Table I. Such an increase in the meta I extinction at 380 nm with increasing temperature was also reported by Lewis et al. (1981) and is consistent with the blue shift of the meta I–meta II isosbestic with increasing temperature reported by these authors. Their conclusion was based on trends in the apparent amplitudes of each component of the derived triple-exponential function which was used to describe their kinetic observations made at numerous monitoring wavelengths. The observation at 380 nm reported in the present study are also best described by the sum of three exponentials. Interpretation of this triple-exponential behavior via the branched meta II model has permitted explicit definition of individual rate constants and relative extinction coefficients of all species contributing to the kinetic absorbance at 380 nm, and suggests that the temperature-induced blue shift of the meta I–meta II isosbestic observed by Lewis et al. (1981) is due to an increase in extinction in the short wavelength side of the meta I absorption band. This observation is supported by the deconvoluted meta I and meta II spectral profiles. The changes observed in the deconvoluted meta I equilibrium spectra with increasing temperature indicate that the increase in extinction at 380 nm is due to a broadening of the blue side of this absorption band (see Figure 5) and a blue shift of the peak of ca. 2 nm over the temperature range studied. In contrast, the deconvoluted equilibrium meta II band was relatively narrow and symmetric at all temperatures. Thus, three independent sets of measurements [the kinetic and equilibrium measurements reported here and the multiple wavelength kinetic measurements of Lewis et al. (1981)] indicate a temperature-induced increase on the blue side of the meta I absorbance band. The peak position and band shape of chromophore absorbance are determined by its interaction with specific opsin amino acid side chains (Honig & Ebrey, 1982). A temperature-sensitive repositioning of one or more of the amino acid side chains responsible for the meta I opsin shift could account for this unexpected observation. Over the temperature range of this study, a temperature-induced modification of the absorption band of stable, unbleached rhodopsin would be surprising. However, in the transient photointermediate meta I, the amino acid side chain configuration which produces the opsin shift is less stable, making it more likely that the meta I retinal absorption could be influenced by temperature.

Interpretation of establishment of the meta I–meta II equilibrium according to the branched meta II model as described here suggests the existence of two discrete energetic forms of meta II distinguishable by their kinetic properties. However, the possibility that there actually exists some continuous distribution of meta II energetic forms, all of which share very similar spectral properties, cannot be ruled out. Interpretation of the dynamics of recombination of carbon monoxide to photodissociated myoglobin at low temperatures have been performed by application of a distributed kinetics

model (Austin et al., 1974). The bacteriorhodopsin photocycle (Xie et al., 1985) and intramolecular proton pumping by bacteriorhodopsin (Rayfield, 1986) have also been considered in terms of the existence of a distribution of molecular energy levels giving rise to complex kinetics. The branched mechanism proposed in this study may be considered a discrete approximation to such distributed kinetics models. Interpreting within this context suggests that meta II may be a spectral intermediate form of rhodopsin capable of occupying a relatively broad range of structural and energetic states producing kinetic behavior more complex than that of a single exponential. Recent Fourier infrared spectroscopy of photoactivated rhodopsin indicates that considerable changes in rhodopsin conformation occur on the time scale of meta II formation (deGrip et al., 1988). Such relatively large-scale protein conformational changes associated with going to the meta II spectral form of rhodopsin suggest that this apparently less compact form of the protein may occupy a distribution of structural and energetic states. The results presented here, taken with those of deGrip et al. (1988), are consistent with meta II representing a relatively flexible dynamic state occupying more than a single, discrete energetic state of the protein.

It is known that the lipid bilayer environment of rhodopsin in native bovine rod outer segment disk membranes becomes more disordered as temperature increases (Straume & Litman, 1988). The physical properties of rhodopsin's membrane environment are expected to have an effect on meta I–meta II interconversion. The following paper in this issue (Mitchell et al., 1990) uncouples the effects of temperature and isothermal variation of bilayer physical properties, achieved by lipid compositional variation, on both the overall meta I–meta II equilibrium and the distribution of meta II into fast and slow forms. The branched meta II model is again used to interpret the same complex kinetics, this time in reconstituted rhodopsin-containing, egg phosphatidylcholine–cholesterol vesicles.

Acknowledgments

We thank Dr. M. L. Johnson for the modified Gauss–Newton nonlinear least-squares algorithm employed in all analyses and for many helpful discussions and assistance with analytical and computer-related aspects of this work.

References

Allende, J. E. (1988) *FASEB J. 2*, 2356–2367.
Applebury, M. L. (1984) *Vision Res. 24*, 1445–1454.
Applebury, M. L., Zuckerman, D. M., Lamola, A. A., & Jovin, T. M. (1974) *Biochemistry 13*, 3448–3458.
Austin, R. H., Beeson, K., Eisenstein, L., Frauenfelder, H., Gunsalus, I. C., & Marshall, V. P. (1974) *Phys. Rev. Lett. 32*, 403–405.
Bartlett, G. R. (1959) *J. Biol. Chem. 234*, 466–468.
Dancshazy, Zs., Govindjee, R., & Ebrey, T. G. (1988) *Proc. Natl. Acad. Sci. U.S.A. 85*, 6358–6361.
Emeis, D., Kuhn, H., Reichert, J., & Hofmann, K. P. (1982) *FEBS Lett. 142*, 29–34.
Gilman, A. G. (1987) *Annu. Rev. Biochem. 56*, 615–649.
Hoffmann, W., Siebert, F., Hofmann, K.-P., & Kreutz, W. (1978) *Biochim. Biophys. Acta 503*, 450–461.
Honig, B., & Ebrey, T. G. (1982) *Methods Enzymol. 88*, 462–470.
Johnson, M. L. (1983) *Biophys. J. 44*, 101–106.
Johnson, M. L., & Frasier, S. G. (1985) *Methods Enzymol. 117*, 301–342.
Kuhn, H. (1981) *Cur. Top. Membr. Transp. 15*, 171–201.
Lewis, J. W., Winterle, J. S., Powers, M. A., Kliger, D. S., & Dratz, E. A. (1981) *Photochem. Photobiol. 34*, 375–384.
Litman, B. J., Kalisky, O., & Ottolenghi, M. (1981) *Biochemistry 20*, 631–634.
Lowry, O. H., Rosebrough, N. J., Farr, A. L., & Randall, R. J. (1951) *J. Biol. Chem. 193*, 65–269.
Lozier, R. H. (1982) *Methods Enzymol. 88*, 133–162.
Matthews, R. G., Hubbard, R., Brown, P. K., & Wald, G. (1963) *J. Gen. Physiol. 47*, 215–240.
Metzler, D. E., Metzler, C. M., & Mitra, J. (1986) *Trends Biochem. Sci. (Pers. Ed.) 11*, 157–159.
Mitchell, D. D., Straume, M., Miller, J. L., & Litman, B. J. (1990) *Biochemistry* (following paper in this issue).
Ostroy, S. E. (1977) *Biochim. Biophys. Acta 463*, 91–125.
Parkes, J. H., & Liebman, P. A. (1984) *Biochemistry 23*, 5054–5061.
Rayfield, G. W. (1986) *Biophys. J. 49*, 209a.
Schleicher, A., Kuhn, H., & Hofmann, K. P. (1989) *Biochemistry 28*, 1770–1775.
Smith, H. G., Jr., Stubbs, G. W., & Litman, B. J. (1975) *Exp. Eye Res. 20*, 211–217.
Stoeckenius, W., & Bogomolni, R. A. (1982) *Annu. Rev. Biochem. 52*, 587–616.
Straume, M., & Litman, B. J. (1988) *Biochemistry 27*, 7723–7733.
Stryer, L. (1986) *Annu. Rev. Neurosci. 9*, 87–119.
Xie, A. H., Nagle, J. F., & Lozier, R. H. (1985) *Biophys. J. 47*, 98a.